

Effects of the Biologically Produced Polymer Alginate Acid on Macroscopic and Microscopic Calcite Dissolution Rates

THOMAS D. PERRY, IV,
OWEN W. DUCKWORTH,[†]
CHRISTOPHER J. MCNAMARA,
SCOT T. MARTIN*, AND
RALPH MITCHELL*

Division of Engineering and Applied Sciences, Pierce Hall,
Harvard University, Cambridge, Massachusetts 02138

Dissolution of carbonate minerals has significant environmental effects. Microorganisms affect carbonate dissolution rates by producing extracellular metabolites, including complex polysaccharides such as alginate acid. Using a combined atomic force microscopy (AFM)/flow-through reactor apparatus, we investigated the effects of alginate acid on calcite dissolution. Macroscopic dissolution rates, derived from the aqueous metal ion concentrations, are $10^{-5.5}$ mol m⁻² s⁻¹ for $5 < \text{pH} < 12$ in the absence of alginate acid compared to $10^{-4.8}$ mol m⁻² s⁻¹ in its presence. The AFM images demonstrate that alginate acid preferentially attacks the obtuse steps of dissolution pits on the calcite surface. In pure water, the obtuse and acute steps retreat at similar rates, and the pits are nearly isotropic except under highly acidic conditions. In alginate acid, the acute step retreat rate is nearly unchanged in comparison to water, whereas the obtuse step retreat rate increases with decreasing pH values. As a result, the pits remain rhombohedral but propagate faster in the obtuse direction. To explain these observations, we propose that alginate acid preferentially forms dissolution active surface complexes with calcium atoms on the obtuse step, which results in anisotropic ligand-promoted dissolution.

Introduction

Calcite dissolution impacts environmental, geological, and hydrogeological systems. Calcite is an important reservoir of carbon, and accelerated dissolution of calcite affects global carbon cycling (1), the chemistry of marine systems (2), and the local pH and alkalinity of terrestrial environments (3). Calcite and other carbonates are the primary pH buffer in many natural waters, and calcite dissolution impacts porosity and heterogeneity in aquifers, which leads to hydrologic complexity in reactive transport modeling (4). In terrestrial environments, calcite dissolution partially regulates the fate and transport of anthropogenic pollutants, especially heavy metals (5–11). Additionally, many stone cultural heritage materials are predominantly calcite in the form of limestones

and marble, and retarding deterioration is important for preserving these irreplaceable artifacts (12). Our understanding of the role of microorganisms in calcite dissolution remains underdeveloped, which is an essential shortcoming of any quantitative prediction of calcite weathering.

Bacteria, Archaea, cyanobacteria, algae, fungi, and lichens stimulate calcite dissolution through production of metabolic by-products, including organic acids and exopolysaccharides (EPS) (13, 14). The exudates are produced by microorganisms in biofilms, which are heterogeneous communities of microorganisms attached to the stone surface in an anchoring matrix of excreted EPS (15). The composition of EPS is genotypically, phenotypically, and environmentally regulated. Its chemical structure varies by microorganism, growth stage, nutrient abundance, and other environmental stimuli (16). The EPS is generally comprised of a variety of sugars, including uronic acids, and often contains functional groups (such as carboxylic acids) that can interact with mineral ions. The specific dissolution effects of EPS depend on mineral type, ligand functionality, acidic moieties, and pH. EPS can impact mineral weathering by a variety of mechanisms (17) and has been demonstrated to either accelerate or retard dissolution rates, although the precise mechanisms and reactions are not well understood (18–20).

EPS polymers are complex macromolecules and difficult to study. These polymers are built up from monomeric units, and the study of these simpler units provides some important insights. For example, although literature reports on the effects of simple organic polydentate ligands on calcite dissolution are sparse, it appears that the distinctive dissolution effects of ligands depend strongly on their chemistry. Chelating agents, including polyaspartic acid (PASP), ethylenediamine tetraacetic acid (EDTA), diethylenetriaminepentaacetic acid (DTPA), and 1,2-cyclohexanediaminetetraacetic acid (CTDA), increase the dissolution rate (21, 22). Many biologically derived compounds, however, inhibit dissolution, including lipids and phospholipids (23, 24), proteins (23), humics (25), and other carboxylated compounds (21, 22), though the effect varies widely with chemical identity and aqueous conditions (26, 27). Polysaccharides, the dominant EPS constituent, have been observed to bind to cations on mineral surfaces, both inhibiting and promoting dissolution (18, 20). However, to our knowledge, there are no previous studies investigating the effect of polysaccharides on calcite dissolution.

In this study, alginate acid was selected as a model environmental polysaccharide to study the effects of a biologically produced polymer on calcite dissolution, because of its well-characterized chemistry, commercial availability, and its presence in the environment. It is a straight-chain, hydrophilic, colloidal, polyuronic acid composed of guluronic (G) and mannuronic (M) acid residues configured in poly-G, poly-M, or alternating GM blocks, all of which are capable of chelating aqueous cations (e.g., Figure 1 of ref 28). Approximately 20–50% of polysaccharides produced in a wide sampling of marine and terrestrial bacteria were uronic acids (29). Alginate acid is a dominant environmental polymer produced by seaweed in marine environments (28) and by the bacterium *Pseudomonas aeruginosa* (30), which is a ubiquitous environmental bacterium (31, 32). Furthermore, it has been demonstrated that alginate acid specifically interacts with crystallographic features of calcite (33) and can increase the dissolution rate of other minerals (34).

The electron donating moieties of the alginate acid polymer, such as carbonyls and hydroxyls, chelate aqueous cations such as Ca²⁺ (Figure 1 of ref 28). The proportion of

* Corresponding author phone: (617)495-2846; fax: (617)496-1471; e-mail: mitchell@deas.harvard.edu.; smartin@deas.harvard.edu.

[†] Current address: Department of Civil and Environmental Engineering, University of California, Berkeley, CA 94720.

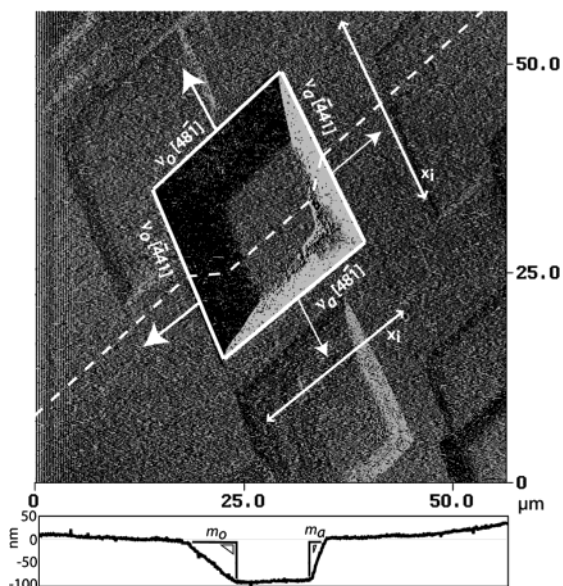


FIGURE 1. Deflection-mode atomic force micrograph of calcite surface after 40 min exposure to 0.1% (w/w) alginic acid at pH 6.8. The hashed white line depicts the pit shape in the z-direction, as shown in a cross section below the micrograph.

M and G sugar residues and their macromolecular conformation determine the physical properties and the affinity of the polymer for cation binding (35). The carboxyl functional groups of poly-G alginates have appropriate spacing and geometry for cation binding (36), and poly-G alginates have a higher affinity for divalent cation binding than their poly-M counterparts (37). The buckled model of poly-G conformation explains the greater binding. An egg-crate conformation of the guluronic regions of two polymer chains forms around calcium ions (Figure 1 of ref 28 (38)). Planar poly-M blocks also bind calcium, although the binding is less ordered than poly-G regions (39) because they do not have the correct spatial and geometric arrangement for chelation sites (40).

To refine our understanding of the chemistry of EPS-mineral interaction, we investigated the effects of alginic acid on calcite dissolution using a combined atomic force microscopy/flow-through reactor. Calcite dissolution has been extensively studied using atomic force microscopy (AFM) for analysis of the dissolution of single crystals of calcite, as reviewed in ref 41.

Methods

Sample Preparation. Alginic acid (sodium salt; Sigma, St. Louis, MO) was added to deionized water and agitated at room temperature for 1 h until visibly dissolved. The alginic acid was produced by *Macrocystis pyrifera* (kelp) and was comprised of 61% M and 39% G residues. The molecular weight range was 12–80 kD. Nanopure deionized water (18.3 M Ω cm; Barnstead, Dubuque, IA) was used for all solutions, which were either purged with purified argon for 2 h or allowed to equilibrate with the atmosphere. The solutions were set to the desired pH with HCl (EM OmniTrace grade) and NaOH (99.998%; Aldrich, St. Louis, MO). The effects of dissolved carbonate and ionic strength on the dissolution rates were assumed negligible (42, 43).

Natural samples of calcite (variety Iceland Spar, Chihuahua, Mexico; Ward's Natural Science, Rochester, NY) were freshly cleaved with a razor blade along the {1014} cleavage plane and affixed to a steel sample holder with dental wax, which provided a fluid barrier to all sides except the desired top face.

Measurement of Macroscopic Dissolution Rates. Samples were placed in an AFM fluid cell apparatus similar to that of Duckworth and Martin (43). Either deionized water or 0.1% (w/w) alginic acid solution at a set pH was pumped through the reaction vessel at a flow rate of 1.0–1.5 mL min⁻¹ (44, 45). Polymer concentrations of 0.1% (w/w) are most likely below local environmental conditions; biofilms in situ are concentrated mats of EPS, whereas the EPS in our system was dilute enough to remain solvated. In terrestrial environments, polysaccharides are the second most abundant organic species following humic substances. In some cases, polysaccharides range from 5 to 30% of the total organic matter (46). Based on calculations performed in MINEQL+ (Environmental Research Software, Hallowell, ME), all experiments were undersaturated with respect to calcite at pH < 11.

The AFM chamber was utilized as a flow-through reactor to determine dissolution rates (42, 43). Rate calculations in the presence of alginic acid in this study are specific to the ratio of monomers (35) and may vary with structure and composition of polymer due to the complexity and irregular repetition of chelating moieties. Effluent fractions were collected in five-minute intervals, yielding at least 10 samples. Samples were analyzed for calcium by graphite furnace atomic absorption spectroscopy (GF-AAS) and flame atomic absorption spectroscopy (F-AAS). A macroscopic dissolution rate (R_{mac} , mol m⁻² s⁻¹) was calculated with the relationship (42)

$$R_{mac} = \frac{q(\Delta[\text{Ca}^{2+}])}{A} \quad (1)$$

where $\Delta[\text{Ca}^{2+}]$ was the change in aqueous concentration (M) of calcium in the solution during the reaction with calcite, q was the flow rate (L s⁻¹), and A was the geometric surface area (m²) of the mineral sample. The geometric surface area of the sample was calculated by taking a digital photograph and comparing the number of pixels on the top face of the crystal to that of the puck, which had a known surface area of 1.77×10^{-4} m². Although our assumption of a flat surface without small-scale irregularities in the topographical features of the sample increased the apparent dissolution rate (42, 47), it did not affect the magnitude of the differences between recorded dissolution rates. Further contributing to our error estimate, the AAS exhibited an analytical error of 10% in comparison to known standard concentrations in the range of 10 nM–2 mM.

Calcium concentration, as an impurity in the alginic acid, was 20-fold greater than that released by the calcite during reaction, and resulted in a poor signal-to-noise ratio. Even so, spike recovery control experiments with alginic acid solutions indicated that the calcium released during dissolution was sufficient to be detected reliably. Furthermore, experiments with protonated and dialyzed alginic acids gave similar results. The calcium recovery methods were further supported by the microscopic dissolution experiments, which showed similar dissolution rates to the macroscopic dissolution experiments.

Microscopic Measurements and Analysis. A Nanoscope IIIa Multimode scanning probe microscope (Digital Instruments, Woodbury, NY) was operated in contact mode with oxide-sharpened silicon nitride probes (nominal radius of curvature of 5–40 nm, force constant of 0.12 N m⁻¹, Digital Instruments). A geometric analysis of a time series of AFM topographic micrographs collected in the same scan direction was used to calculate a microscopic dissolution rate, R_{mic} (mol m⁻² s⁻¹). The volume of material removed from the calcite surface was calculated by tracking pit growth (Figure 1). The average step retreat rate (v_{avg} , m s⁻¹) for an

expanding pit on the mineral surface was determined using the following equation:

$$v_{avg} = \frac{1}{2} \frac{1}{\tau} \frac{\sum_i \Delta x_i}{2(N-1)} \quad (2)$$

where Δx_i was the change in a lateral pit dimension, τ was the time between consecutive images, and N was the number of images in the series (43).

The microscopic dissolution rate (R_{mic}) was calculated by multiplying the average step retreat rate by the characteristic slope of the surface (42, 43, 47)

$$R_{mic} = \frac{v_{avg}(\Delta h)}{V_M(\Delta l)} \quad (3)$$

where V_M was the molar volume ($\text{m}^3 \text{mol}^{-1}$). The characteristic slope of the surface ($\Delta h/\Delta l$) was calculated by multiplying the total step length by the step height in a defined unit area ($> 40 \times 40 \mu\text{m}^2$), thereby estimating the surface step density (42, 43, 47).

On the atomic scale, the out-of-plane C–O angles of carbonate groups on steps of the (10 $\bar{1}$ 4) calcite face are oriented at different angles on opposite sides of the rhombohedral pits, viz. in obtuse and acute directions (Figures 1, 4, and 6). The differences in C–O orientations lead to anisotropic dissolution (44, 48, 49), with step retreat typically occurring more rapidly for the obtuse step (42, 44, 50). The arithmetic average step retreat rate is obtained as follows

$$v_{avg} = \frac{(v_o + v_a)}{2} \quad (4)$$

from the obtuse (v_o) and acute (v_a) step retreat rates. Measurements of v_{avg} were validated by determining step retreat rate using two separate methods, when possible. (1) Step retreat rate was calculated in relationship to a fixed point (such as a surface contaminant). (2) Step retreat rate was calculated by expansion of two opposing pit walls (22). Further experimentation depended primarily on method two.

The relationship of step slope to step retreat rate is as follows

$$\frac{m_o}{m_a} = \frac{v_a}{v_o} \quad (5)$$

where m_o and m_a are, respectively, the obtuse and acute slopes of the microscopic pit walls (Figure 1) (47, 49, 51). Measurements of v_{avg} , m_o , and m_a combined with eqs 4 and 5 yielded the individual step retreat rates v_o and v_a .

Alginic Acid Surface Attachment. The binding of alginic acid to the mineral surface was investigated using a polysaccharide stain and visible light microscopy. Deionized water was pumped through a flow cell (Biosurface Technologies, Bozeman, MT) mounted on a light microscope (BX60 Olympus, Melville, NY) containing a small piece of calcite prepared similarly to the above protocol. The calcite was imaged (Spot RT digital camera, Diagnostic Instruments, Sterling Heights, MI) with water and alginic acid using a 1% (w/w) solution of the polysaccharide stain alcian blue (Polysciences, Inc., Warrington, PA).

Results and Discussion

Macroscopic Dissolution Rate and Mechanistic Model.

A mechanistic model has been applied successfully to rationalize calcite dissolution rates in water (52, 53). According to the model, far from equilibrium the dissolution of calcite

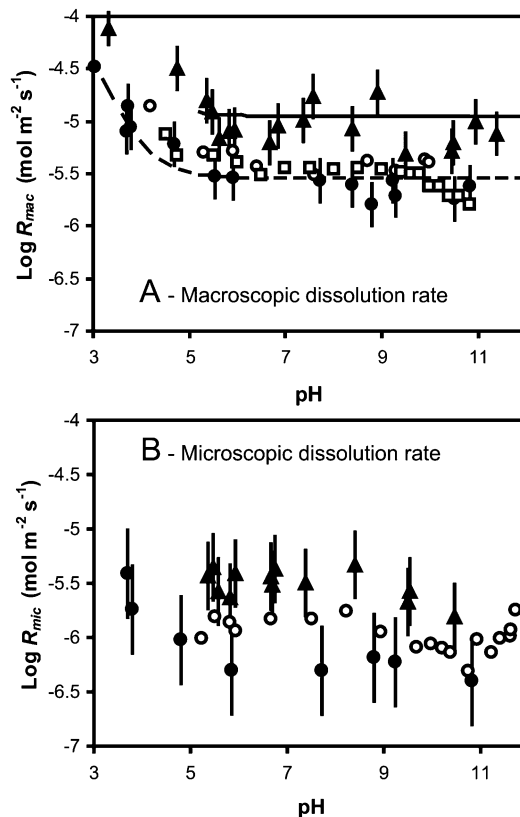
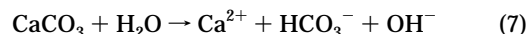
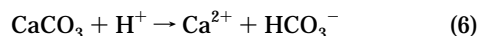


FIGURE 2. (A) Macroscopic (eq 1) and (B) microscopic (eq 3) log dissolution rates. Key: 0.1% (w/w) alginic acid (▲), deionized water in this work (●), ref 42 (○), and ref 53 (□). Lines show fit to mechanistic models for water (eq 8, - -) and alginic acid (eq 9, -).

in aqueous solutions occurs via proton- and water-promoted reactions:



The dissolution rate is given by

$$R_{diss} = k_1[\text{H}^+] + k_2[\text{H}_2\text{O}] \quad (8)$$

where k_1 and k_2 are rate coefficients and $[\text{H}_2\text{O}] = 1$. For our reactions in deionized water, the rate coefficients are empirically solved as $k_1 = 10^{-1.46} \text{M}^{-1} \text{mol m}^{-2} \text{s}^{-1}$ and $k_2 = 10^{-5.54} \text{mol m}^{-2} \text{s}^{-1}$ for calcite, which are consistent with literature reports (Figure 2A) (41).

Over the entire range of pH values investigated ($3.3 < \text{pH} < 11.4$), alginic acid increased the dissolution rate by approximately 6-fold (Figure 2A). The enhancement is described in the mechanistic model as an additional pathway due to ligand-promoted dissolution by alginic acid:

$$R_{diss} = k_1[\text{H}^+] + k_2[\text{H}_2\text{O}] + k_3[\text{alginic acid}] \quad (9)$$

In circumneutral and alkaline regimes under our experimental conditions, the alginic acid pathway exceeds the water promoted rate ($k_3 = 10^{-4.95} \text{mol m}^{-2} \text{s}^{-1} \text{g}^{-1} \text{L}$). The mechanistic model was not extended for $\text{pH} < 5$ because of difficulties in collecting data due to fast reaction rates. Even so, the data qualitatively suggest that alginic acid increases the dissolution rate for $\text{pH} < 5$.

For $\text{pH} < 3$, mechanistic models overpredict dissolution rates because they do not account for the effect of surface charging on proton adsorption (43, 54). Although the data

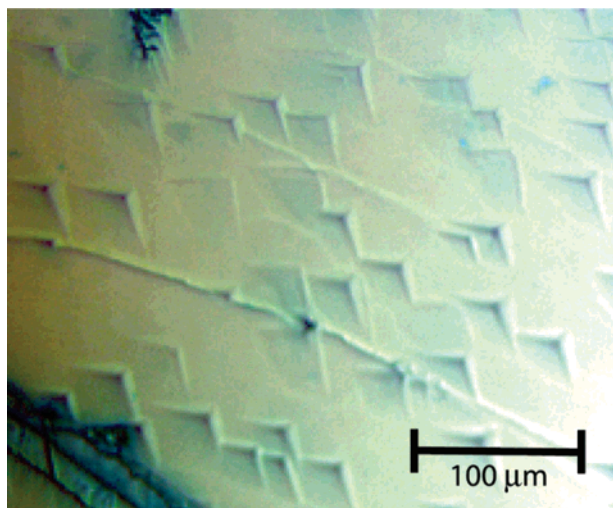


FIGURE 3. Optical microscope color image (100X) of alginic acid stained by alcian blue on calcite at pH 5.6. Polymers accumulate on the rough areas of the crystal surface. There is a thin film of alginic acid across the surface with pockets of increased alginate accumulation in pits, which may be the result of preferential accumulation or hydrodynamics.

are few at low pH, the apparent increase in dissolution rate in the presence of alginic acid suggests that the polymer–mineral interaction changes. Proton mass-transport kinetics

no longer limits the reaction rate, supporting the hypothesis of an independent alginic acid mechanism (53, 55). The optical microscopy experiments confirm that thick alginate gels do not form on the calcite surface, which might otherwise affect the surface reaction environment and hence dissolution rates (37).

The applicability of eq 9 is limited because the alginic acid adsorption and dissolution reactions are coupled in k_3 . This adsorption term may result in some variability in the rate coefficient as a function of pH and [alginic acid]. Therefore, it is preferable to relate the dissolution rate to the concentration of alginic acid adsorbed to the surface, as follows

$$R_{diss} = k_1[H^+] + k_2[H_2O] + k_3'\theta[\text{alginic acid}]_{\text{surf}} \quad (10)$$

where θ is the fractional surface coverage by alginic acid and k_3' is the dissolution rate coefficient of the adsorbed alginic acid species. The ability to determine molecular coverage would allow separate descriptions of alginic acid adsorption and dissolution. At sufficient alginic acid concentrations, $\theta = 1$ in the saturation regime of the adsorption isotherm (4). The optical microscope observations with stain in continuous flow demonstrate the adsorption of alginic acid on the calcite surface (Figure 3) and are consistent with complete surface coverage. Irreversible sorption of the polymer to the calcite surface is possible. However, at the dissolution active sites (e.g., pits) morphological change is observed indicating

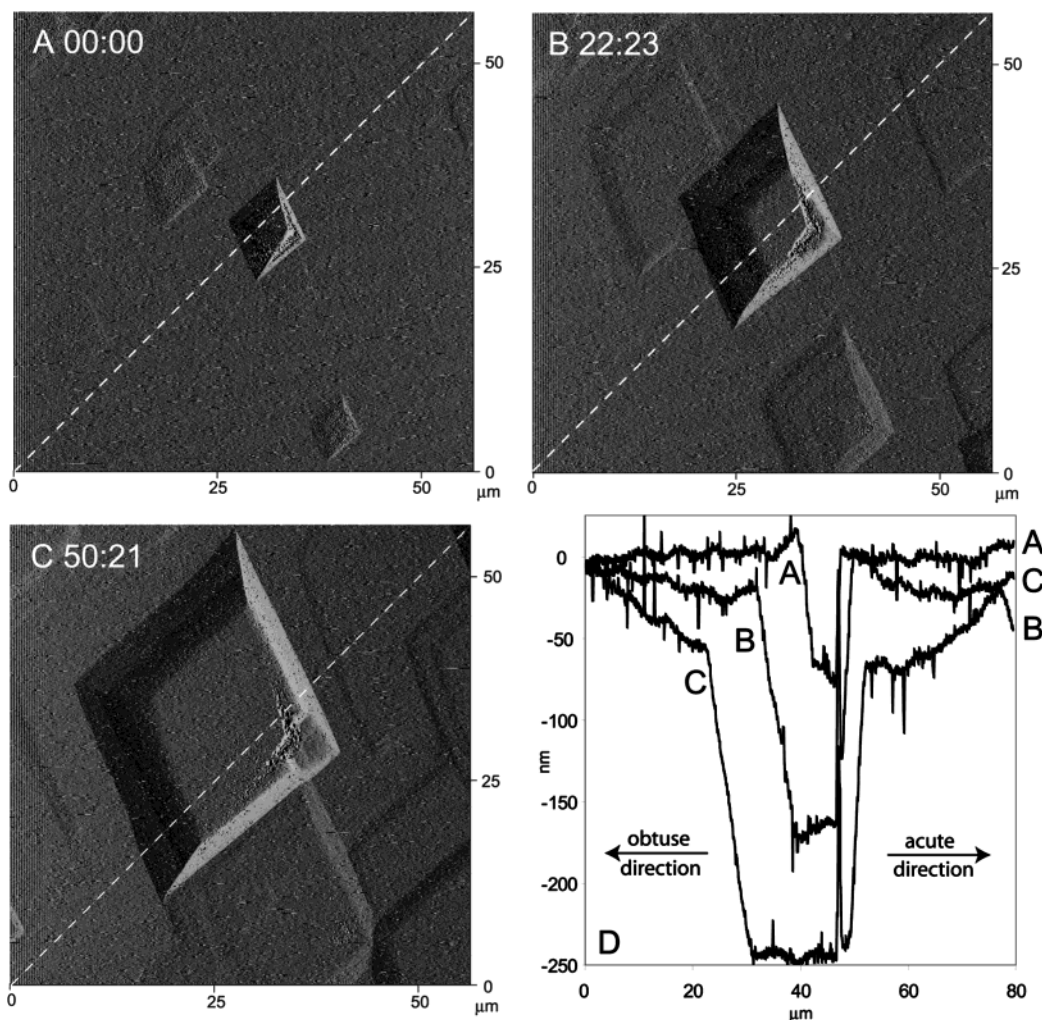


FIGURE 4. (A–C) Time series deflection-mode atomic force micrographs of calcite surface during exposure to 0.1% (w/w) alginic acid at pH 6.8. Hashed lines are cross sections (shown in D) of height-mode micrographs. Pits are in the same orientation as Figure 1.

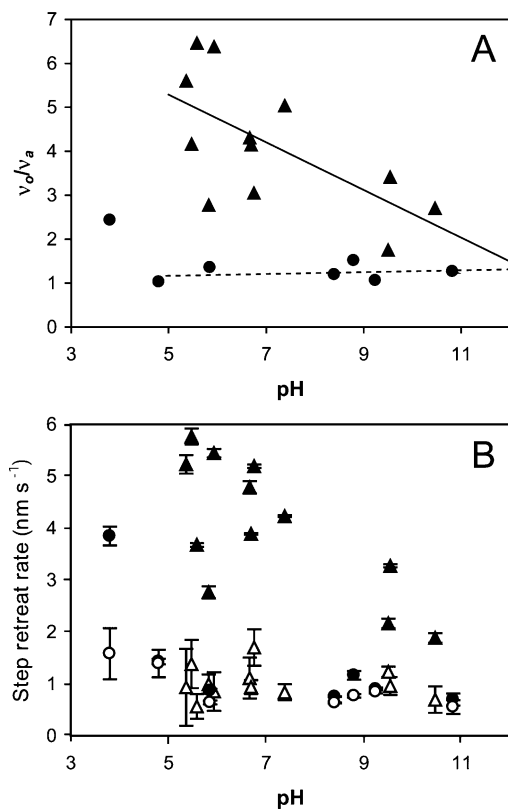


FIGURE 5. (A) Step retreat ratio (v_d/v_a) for alginic acid (▲) and deionized water (●) with best-fit lines. (B) Obtuse (▲) and acute (△) step retreat rates for 0.1% (w/w) alginic acid. Same for deionized water (●, ○).

material turnover. Based on these observations, we take $\theta = 1$, and k_3' is thus $10^{-4.95} \text{ mol m}^{-2} \text{ s}^{-1}$.

Microscopic Dissolution Rates. A time series of micrographs and cross-sectional analysis of pit depth (Figure 4) show calcite dissolution in the presence of alginic acid. Microscopic dissolution rates calculated from the step retreat

rates demonstrate that alginic acid increases the dissolution rate compared to control experiments for $5.4 < \text{pH} < 10.5$ (Figure 2B). Both in the presence and absence of alginic acid, dissolution occurs by formation of pits that expand laterally and deepen into the crystal surface. For trials with alginic acid, analyses of the microscopic dissolution rate were not performed for $\text{pH} < 5$ because the step retreat rates were too rapid for image capture. Step retreat rates in the absence of alginic acid agree with published reports, using both similar (42, 49, 56, 57) and different (41, 58) experimental apparatus.

The macroscopic and microscopic dissolution rates (R_{mac} and R_{mic}) agree reasonably well, both in the absence ($R_{mac}/R_{mic} = 4.21 \pm 1.46$) and in the presence ($R_{mac}/R_{mic} = 2.84 \pm 0.82$) of alginic acid. Duckworth and Martin (47) address the issue of $R_{mac}/R_{mic} > 1$ for the combined flow-through/microscopic dissolution analytical technique. The good agreements of R_{mac} with R_{mic} validates using these measurement techniques when experimenting with complex biological polymers.

The accuracy of the microscopic dissolution rate is affected by the uncertainty in the measurement of the characteristic slope of the surface. The average characteristic surface slope in the absence of alginic acid was 0.03 ± 0.01 , compared to 0.05 ± 0.01 in the presence of alginic acid. The increase occurs because the pits in the alginic acid exposure were generally deeper than those in its absence, causing increases in the surface roughness, the step density, and the characteristic surface slope.

Differences in Obtuse and Acute Step Retreat Rates. In the absence of alginic acid, obtuse and acute step retreat rates are nearly equal for $\text{pH} > 5$, though they become increasingly different at lower pH values (Figure 5A). This observation has also been reported for other carbonate minerals (43, 47). At low pH values, we observed an increased obtuse step retreat rate, in disagreement with Di Giudici (59), who employed a slower flow rate (0.06 mL min^{-1}).

Pits formed in the presence of alginic acid solutions expand rapidly in the obtuse directions (Figure 4D), implicating interaction of the alginic acid with the mineral surface. The effect of alginic acid was repeatedly confirmed by comparing obtuse and acute pit step retreat rates for multiple

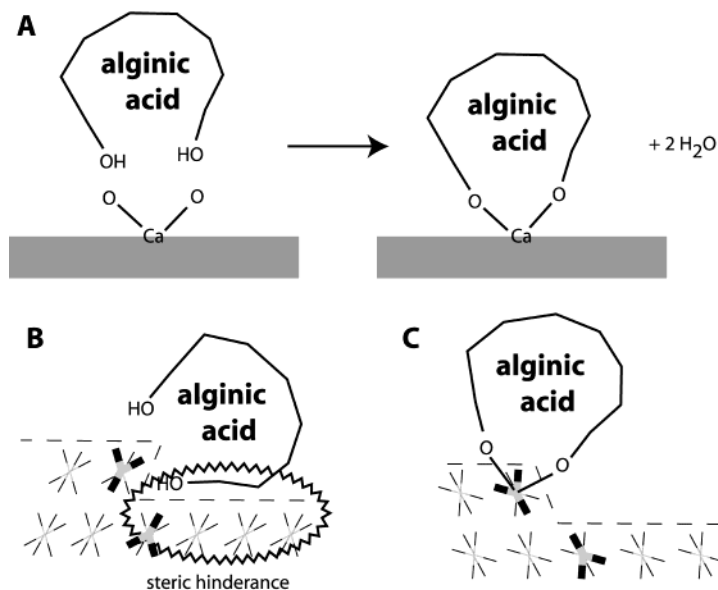


FIGURE 6. A. Ligand-promoted dissolution of calcite involving bidentate chelation by carbonyls/hydroxyls of alginic acid to surficial calcium. Two protons (not shown) are also necessary in the stoichiometry of this reaction. B. On acute steps, the approach of the alginic acid ligand moieties is hypothesized to be sterically hindered. C. In contrast, cations on the obtuse step are exposed. We hypothesize that the Ca^{2+} on the obtuse step is chelated by the electron-donating moieties of the alginic acid and rapid dissolution ensues. (Note: figure is not drawn to scale.)

experimental conditions (Figure 5A,B). The effect of image drift was negligible because the expansion of two opposing pit walls was measured and scaled by the step slope (22). The effect was strongly pH dependent, which may be the result of the increasing importance of proton-promoted dissolution at decreasing pH. The data variability apparent in Figure 5 is likely due to the effect of alginic acid and mineral surface heterogeneity on microscopic observations.

Surficial Cation Chelation. Because the dissolution rate in the presence of alginic acid is increased by a similar magnitude at all pH values, an additional mechanism beyond proton (eq 6) or water promoted (eq 7) reactions is indicated. During interaction with a mineral surface containing calcium ions, the alginic acid may chelate surficial cations from the crystal (Figure 6A) (60), causing ligand-promoted dissolution. In a nucleophilic attack, the electron-donor moieties (carbonyls and hydroxyls) of the alginic acid replace the water associated with surficial calcium (42). The association of polymer ligand and mineral cations results in electron withdrawal between the surficial calcium and the carbonates in the mineral lattice, resulting in polarized bonds (60), thereby facilitating ligand-promoted dissolution.

Alginic acid increases the dissolution rate through preferential ligand-promoted dissolution on the obtuse pit step. The preferential attack on the obtuse step may be the result of steric hindrance of alginic acid binding groups imposed by the acute step (Figure 6B). Moreover, cations on the obtuse step are relatively exposed in comparison to the acute step (Figure 6C). On the acute step, portions of the carbonate species protrude from the pit edge and may decrease the possibilities of the chelating moieties to contact the surficial cations (Figure 6B). This selective dissolution mechanism and thereby the structure–function relationship of the polymer and mineral surface is important in understanding the effect of these polymers.

Environmental Implications. Alginic acid is a single polymer in a diverse array of environmental polymers. The dissolution effects of EPS are distinctive to the chemical nature of the polymer, as demonstrated by the varied observed effects in the literature. However, there are several possible mechanisms whereby alginic acid could have an even greater effect in situ over-and-above the effects observed in the laboratory experiments employed in this study. The additional in situ mechanisms and effects are considered below.

The dissolution rate can be expressed in terms of aqueous saturation (S) by the following eq (61):

$$R = k(1 - S) \quad (11)$$

This governing equation is useful for considering a variety of additional effects of the polymers under environmental conditions. Because of the ability of EPS constituents to bind aqueous calcium ions, it decreases S , thereby increasing the dissolution rate. Polysaccharides also provide nucleation sites for secondary precipitates, including calcite-bearing precipitates (62). The removal of aqueous calcium accompanying secondary precipitation reduces S and thus increases the calcite dissolution rate of substrate calcite as in eq 11 (63, 64). Polysaccharide gels are composed of 90–99% water and act as an antidesiccant, which helps to maintain a medium for diffusion even as water potential decreases. Hence S increases (65), which increases the time the surface is in an aqueous environment conducive to mineral dissolution even under arid conditions (17). Polysaccharides are also complex and thereby sequester other metal ions, such as manganese and magnesium, that would otherwise inhibit calcite dissolution (39, 49, 66). These other mechanisms suggest our results are the minimum effect of EPS polymers in situ (34).

In summary, alginic acid causes an increase in the dissolution rate of calcite across a range of pH values. The proposed mechanism for enhancement is preferential obtuse step surface chelation of calcium that, through bond polarization, reduces the activation energy required for breaking lattice bonds and thereby increases the dissolution rate.

Acknowledgments

This work was supported in part by a Samuel H. Kress Foundation fellowship to T.D.P., a Sandia National Laboratories Campus Executive Fellowship to O.W.D., support from the New York Community Trust Merck Fund and from the Chemical Sciences, Geosciences, and Biosciences Division, Office of Basic Energy Sciences, Office of Science, U.S. Department of Energy to S.T.M., and a grant from the National Science Foundation (number BES-9906337) and support from the W. R. Grace Corporation to R.M. The authors are grateful for helpful conversations with T. A. Kendall and H.-M. Hung.

Supporting Information Available

Tabulated data for macroscopic and microscopic dissolution rates, rate comparison, step retreat rates, and pit anisotropy in water and alginic acid solutions. This material is available free of charge via the Internet at <http://pubs.acs.org>.

Literature Cited

- Schlesinger, W. H. *Biogeochemistry: An Analysis of Global Change*, 2nd ed.; Academic Press: San Diego, 1997.
- Pilson, M. *An Introduction to the Chemistry of the Sea*; Prentice Hall: Upper Saddle River, NJ, 1998.
- Stumm, W.; Morgan, J. J. *Aquatic Chemistry*, 3rd ed.; Wiley: New York, 1996.
- Stumm, W. *Chemistry of the Solid-Water Interface*; Wiley: New York, 1992.
- Amirbahman, A.; Schoenberger, R.; Johnson, C.; Sigg, L. *Environ. Sci. Technol.* **1998**, *32*, 1933–1940.
- Stipp, S. L.; Konnerup-Madsen, J.; Franzreb, K.; Kulik, A.; Mathieu, H. *Nature* **1998**, *396*, 356–359.
- Hoffman, U.; Stipp, S. L. *Geochim. Cosmochim. Acta* **2001**, *65*, 4131–4139.
- Warren, L.; Maurice, P.; Parmar, N.; Ferris, F. *Geomicrobiology* **2001**, *18*, 93–115.
- Reeder, R. J.; Nugent, M.; Tait, C.; Morris, D.; Heald, S.; Beck, K.; Hess, W.; Lazirotti, A. *Geochim. Cosmochim. Acta* **2001**, *65*, 3491–3503.
- Elzinga, E.; Reeder, R. J. *Geochim. Cosmochim. Acta* **2002**, *66*, 3943–3954.
- Elzinga, E.; Reeder, R. J.; Withers, S.; Peale, R.; Mason, R.; Beck, K.; Hess, W. *Geochim. Cosmochim. Acta* **2002**, *66*, 2875–2885.
- Saiz-Jimenez, C. *Geomicrobiol. J.* **1999**, *16*, 27–37.
- Perry, T. D.; McNamara, C. J.; Mitchell, R. *Proc. Nat. Acad. Sci.* Submitted for publication.
- Christensen, B. E.; Characklis, W. G. In *Biofilms*; 1st ed.; Characklis, W. G., Marshall, K. C., Eds.; Wiley: New York, 1990; pp 93–130.
- Costerton, J. W.; Stewart, P. S.; Greenberg, E. P. *Science* **1999**, *284*, 1318–1322.
- Christensen, B. E.; Characklis, W. G. In *Biofilms*; Characklis, W. G., Marshall, K. C., Eds.; Wiley: New York, 1990.
- Barker, W. W.; Welch, S. A.; Banfield, J. F. *Rev. Mineral.* **1997**, *35*, 391–428.
- Welch, S. A.; Vandevivere, P. *Geomicrobiol. J.* **1994**, *12*, 227–238.
- Banfield, J. F.; Barker, W. W.; Welch, S. A.; Taunton, A. *Proc. Natl. Acad. Sci. U.S.A.* **1999**, *96*, 3404–3411.
- Flemming, H. C.; Wingender, J. *Water Sci. Technol.* **2001**, *43*, 9–16.
- Fredd, C.; Fogler, H. *J. Colloid. Interface. Sci.* **1998**, *204*, 187–194.
- Wu, Y.; Grant, C. *Langmuir* **2002**, *18*, 6813–6820.
- Suess, E. *Geochim. Cosmochim. Acta* **1970**, *34*, 157–168.
- Frye, G.; Thomas, M. *Chem. Geol.* **1993**, *109*, 215–226.
- Hoch, A.; Reddy, M.; Aiken, G. *Geochim. Cosmochim. Acta* **2000**, *64*, 61–72.

- (26) Thomas, M.; Clouse, J.; Longo, J. *Chem. Geol.* **1993**, *109*, 227–237.
- (27) Compton, R. G.; Sanders, G. *J. Colloid. Interface. Sci.* **1993**, *158*, 439–445.
- (28) Davis, T. A.; Llanes, F.; Volesky, B.; Mucci, A. *Environ. Sci. Technol.* **2003**, *37*, 261–267.
- (29) Kennedy, A. F. D.; Sutherland, I. W. *Biotechnol. Appl. Biochem.* **1987**, *9*, 12–19.
- (30) Boyd, A.; Chakrabarty, A. M. *J. Ind. Microbiol.* **1995**, *15*, 162–168.
- (31) Wolfgang, M. C.; Kulasekara, B. R.; Liang, X. Y.; Boyd, D.; Wu, K.; Yang, Q.; Miyada, C. G.; Lory, S. *Proc. Natl. Acad. Sci.* **2003**, *100*, 8484–8489.
- (32) Hardalo, C.; Eddberg, S. C. *Crit. Rev. Microbiol.* **1997**, *23*, 47–75.
- (33) Didymus, J. M.; Oliver, P.; Mann, S.; DeVries, A. L.; Hauschka, P. V.; Westbroek, P. *J. Chem. Soc., Faraday Trans.* **1993**, *89*, 2891–2900.
- (34) Welch, S. A.; Barker, W. W.; Banfield, J. F. *Geochim. Cosmochim. Acta* **1999**, *63*, 1405–1419.
- (35) Haug, A.; Mykestad, S.; Larsen, B.; Smidsrød, O. *Acta Chem. Scand.* **1967**, *21*, 768–768.
- (36) Dheu-Andries, M. L.; Perez, S. *Carbohydr. Res.* **1983**, *124*, 324–332.
- (37) Smidsrød, O.; Haug, A. *Acta Chem. Scand.* **1965**, *19*, 329.
- (38) Rees, D. A. *Pure Appl. Chem.* **1981**, *53*, 1–14.
- (39) Braccini, L.; Grasso, R. P.; Perez, S. *Carbohydr. Res.* **1999**, *317*, 119–130.
- (40) Grant, G. T.; Morris, E. R.; Rees, D. A.; Smith, P. J. C.; Thom, D. *FEBS Lett.* **1973**, *32*, 195–198.
- (41) Arvidson, R. S.; Ertan, I. E.; Amonette, J. E.; Luttge, A. *Geochim. Cosmochim. Acta* **2003**, *67*, 1623–1634.
- (42) Shiraki, R.; Rock, P. A.; Casey, W. H. *Aquat. Geochem.* **2000**, *6*, 87–108.
- (43) Duckworth, O. W.; Martin, S. T. *Geochim. Cosmochim. Acta* **2003**, *67*, 1787–1801.
- (44) Liang, Y.; Baer, D. R. *Surf. Sci.* **1997**, *373*, 275–287.
- (45) Sjöberg, E.; Rickard, D. *Geochim. Cosmochim. Acta* **1983**, *47*, 2281–2286.
- (46) Martin, J. P. *Soil Biol. Biochem.* **1971**, *3*, 33–41.
- (47) Duckworth, O. W.; Martin, S. T. *Am. Min.* **2004**, *89*, 554–563.
- (48) Hillner, P. E.; Gratz, A. J.; Manne, S.; Hansma, P. K. *Geology* **1992**, *20*, 359–362.
- (49) Lea, A. S.; Amonette, J. E.; Baer, D. R.; Liang, Y.; Colton, N. G. *Geochim. Cosmochim. Acta* **2001**, *65*, 369–379.
- (50) Jordan, G.; Rammensee, W. *Geochim. Cosmochim. Acta* **1998**, *62*, 941–947.
- (51) Liang, Y.; Baer, D. R.; McCoy, J. M.; LaFemina, J. P. *J. Vac. Sci. Technol. A-Vac. Surf. Films* **1996**, *14*, 1368–1375.
- (52) Chou, L.; Garrels, R. M.; Wollast, R. *Chem. Geol.* **1989**, *78*, 269–282.
- (53) Busenberg, E.; Plummer, L. N. *U.S. Geol. Surv. Bull.* **1986**, *1578*, 139–168.
- (54) Pokrovsky, O. S.; Schott, J. *Geochim. Cosmochim. Acta* **1999**, *63*, 881–897.
- (55) Sjöberg, E.; Rickard, D. *Chem. Geol.* **1984**, *42*, 119–136.
- (56) Liang, Y.; Baer, D. R.; McCoy, J. M.; Amonette, J. E.; LaFemina, J. P. *Geochim. Cosmochim. Acta* **1996**, *60*, 4883–4887.
- (57) Hong, Q.; Suarez, M. F.; Coles, B. A.; Compton, R. G. *J. Phys. Chem. B* **1997**, *101*, 5557–5564.
- (58) MacInnis, I. N.; Brantley, S. L. *Geochim. Cosmochim. Acta* **1992**, *56*, 1113–1126.
- (59) Di Giudici, G. *Am. Miner.* **2002**, *87*, 1379–1285.
- (60) Duckworth, O. W.; Martin, S. T. *Geochim. Cosmochim. Acta* **2001**, *23*, 4289–4302.
- (61) Plummer, L. N.; Packhurst, D. L.; Wigley, T. L. M. *Am. J. Sci.* **1978**, *278*, 179–219.
- (62) Urrutia, M.; Beveridge, T. *Chem. Geol.* **1994**, *116*, 261–280.
- (63) Sjöberg, E. *Geochim. Cosmochim. Acta* **1976**, *40*, 441–447.
- (64) Morse, J. W.; Berner, R. A. *Am. J. Sci.* **1972**, *272*, 840–851.
- (65) Chenu, C.; Roberson, E. *Soil Biol. Biochem.* **1996**, *28*, 877–884.
- (66) Compton, R. G.; Brown, C. *J. Colloid. Interface. Sci.* **1994**, *165*, 445–449.

Received for review November 22, 2003. Revised manuscript received March 3, 2004. Accepted March 11, 2004.

ES035299A